JOURNAL OF AIRCRAFT
Vol. 34, No. 6, November–December 1997

In-Flight Boundary-Layer State Measurements on a High-Lift System: Main Element and Flap

C. P. van Dam* and S. M. Los†
University of California, Davis, Davis, California 95616
S. J. Miley‡
Old Dominion University, Norfolk, Virginia 23508
V. E. Roback§ and L. P. Yip¶
NASA Langley Research Center, Hampton, Virginia 23681
A. Bertelrud**
Analytical Services and Materials, Inc., Hampton, Virginia 23666
and
P. M. H. W. Vijgen††
High Technology Corporation, Hampton, Virginia 23666

Flight experiments on NASA Langley Research Center's B737-100 airplane were conducted to document flow characteristics for further understanding of the flow physics on multielement high-lift systems. The measurements presented in this paper show that significant regions of laminar flow exist on the main element and the foreflap of the airplane. Flow mechanisms that affect the extent of laminar flow include relaminarization of the flow in the leading-edge region of the main element and contamination of the laminar flow on the flap by turbulent shear layers emanating from upstream elements. This information should be valuable in the development and assessment of high-Reynolds-number wind-tunnel experiments and numerical models for predicting the flows around multielement wings at full-scale high-lift conditions.

Nomenclature

C_p = pressure coefficient, $(p - p_\infty)/q_\infty$
$C_{p,\max}$ = maximum pressure coefficient in leading-edge region of main element
c = local chord length, ft
$\bar{c}$ = mean aerodynamic chord, 11.20 ft
h_p = pressure altitude, ft
K = relaminarization parameter
M_∞ = freestream Mach number
p = local static pressure, psf
p_∞ = freestream static pressure, psf
q_∞ = freestream dynamic pressure, psf
R_{bar} = attachment-line Reynolds number
$R_{\bar{c}}$ = Reynolds number, $V_\infty \bar{c}/\nu$
s = surface distance, ft
t = time, s
V_i = indicated airspeed, kn
V_∞ = true airspeed, ft/s
x/c = nondimensional chordwise coordinate
z/c = nondimensional thickness coordinate
α = airplane angle of attack, deg
γ = turbulent intermittency factor
δ_f = flap setting, deg
Λ = wing sweep angle, deg
ν = kinematic viscosity, ft^2/s

Presented as Paper 95-3911 at the AIAA 1st Aircraft Engineering, Technology, and Operations Congress, Los Angeles, CA, Sept. 19–21, 1995; received Jan. 16, 1997; revision received May 27, 1997; accepted for publication May 30, 1997.

*Professor, Department of Mechanical and Aeronautical Engineering. E-mail: cpvandam@ucdavis.edu. Senior Member AIAA.
†Graduate Student, Department of Mechanical and Aeronautical Engineering.
‡Senior Research Associate. Senior Member AIAA.
§Aerospace Technologist. Member AIAA.
¶Senior Research Engineer. Associate Fellow AIAA.
**Principal Scientist. Senior Member AIAA.
††R&D Engineer; currently Senior Specialist Engineer, Boeing Commercial Airplane Group, Seattle, WA 98124. Senior Member AIAA.

Introduction

THE accurate prediction of the aerodynamic performance of a multielement high-lift system at full-scale flight conditions is a critical part of the design and development process of subsonic civil transport airplanes. However, the combination of complex geometry and flow physics makes the aerodynamic design and analysis of high-lift system at these conditions very challenging. Prediction of full-scale aerodynamic performance from computational fluid dynamics (CFD) is still inaccurate because of deficiencies in modeling of the high-lift flow physics, as well as limitations in computer hardware. Also, the sensitivity of the high-lift flows to variations in Reynolds number makes the prediction of full-scale aerodynamic performance based on wind-tunnel measurements at lower Reynolds numbers difficult, and this extrapolation process requires a complete understanding of the scaling principles.

This lack of capabilities in the prediction of high-lift aerodynamic performance at full-scale Reynolds numbers was partially responsible for the development of high-Reynolds-number wind tunnels[1] and the need for detailed flight measurements at full-scale conditions. In response to the need for carefully documented data on aspects of the flows about full-scale multielement configurations at high-lift conditions, a multiphased flight research project was conducted on the NASA Transport Systems Research Vehicle (TSRV), a Boeing B737-100. The details of this project including relevant publications are presented in a companion paper[2] on the boundary-layer state measurements of the slat. Extended runs

of laminar flow were shown to exist on the slat for nearly the entire angle-of-attack range. One of the unique features of this experiment was that hot-film anemometers were not only installed on the slat (as was the case in the A310 experiment[3,4]), but also on the main element and the foreflap to determine if regions of laminar flow exist downstream of the slat on multielement high-lift wings at full-scale conditions. In two-dimensional wind-tunnel experiments of a three-element airfoil at high Reynolds numbers, it was found that for most of the angle-of-attack range, the main element was laminar forward from the suction peak on the upper surface, and forward from about 75% of its chord on the lower surface.[5] The lower surface of the flap was completely laminar for most of the angle-of-attack range, but on the upper surface, contamination by turbulence caused transition in the strong favorable pressure gradient ahead of the suction peak.[5] Typically, three transition mechanisms are considered in two-dimensional high-lift flows: growth of Tollmien–Schlichting and inflectional instabilities, laminar separation, and contamination by shear layers emanating from upstream elements.[6] In three-dimensional flows, attachment-line contamination and the growth of crossflow instabilities provide additional possible transition mechanisms. Given this multitude of transition mechanisms including possible turbulent contamination of the main element by the slat and the flap by both the slat and the main element, the question of whether or not extended runs of laminar flow can exist on the main element and the flap surfaces of a subsonic transport wing at full-scale conditions arises. Also, in the companion article,[2] relaminarization of the turbulent flow originating at the attachment line was observed in regions with strong favorable pressure gradients. Given this observation, it is questioned whether conditions exist on the main element and the flap that would favor relaminarization.

This paper describes and discusses the boundary-layer state changes that were measured in flight on the main element and the foreflap of NASA Langley Research Center's TSRV (B737-100).

Flight Experiment and Instrumentation

An overview of the test conditions in terms of the Reynolds number and Mach number is given in Ref. 7. The chord Reynolds number (based on freestream conditions and a reference chord of 11.20 ft) and the freestream Mach number ranged from 1×10^7 to 2.5×10^7 and 0.16 to 0.48, respectively. Reference 2 gives detailed descriptions of the test airplane, the installed instrumentation, and the data acquisition system and its accuracy. In this paper, the wing layout and instrumentation pertinent to the measurements on the main element and the foreflap are discussed. Only the starboard wing outboard of the engine was instrumented. In this region, the wing section in the high-lift configuration consists of five elements: the slat, the main element, and three flap elements. There are three outboard slats on the starboard wing identified as slats nos. 4, 5, and 6 (Fig. 1). During takeoff, these slats are deployed in a sealed position, as typified by the sketches for the 5- and 15-deg wing sections in Fig. 2. Beyond a flap setting of 25 deg, slats nos. 5 and 6 are fully extended and deflected to form a gap between the slat and the main element, as typified by the 30- and 40-deg wing sections in Fig. 2. This extra slat deflection creates a spanwise break in the leading edge between slats nos. 4 and 5 for the high-lift system in the landing configuration (Fig. 1). Figure 1 also shows the pressure measurement stations including the pressure belt wrapped around the main element. A pressure belt was used on the main wing

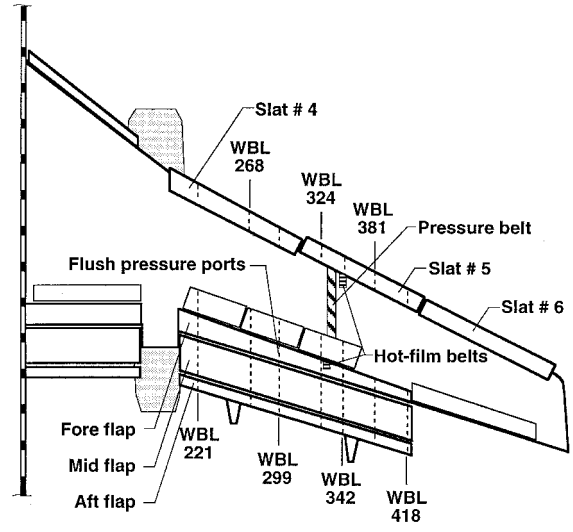

Fig. 1 Layout of pertinent instrumentation on starboard wing of NASA TSRV (B737-100). Wing depicted in landing configuration ($\delta_f > 25$ deg).

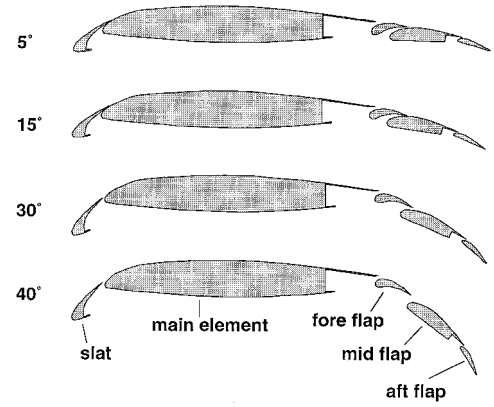

Fig. 2 Wing section geometry for 5, 15, 30, 40 deg (wing segment that includes slat no. 5).

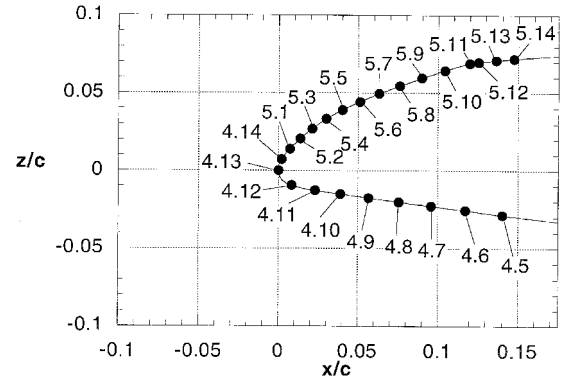

Fig. 3 Location of hot-film sensors in leading-edge region of main element.

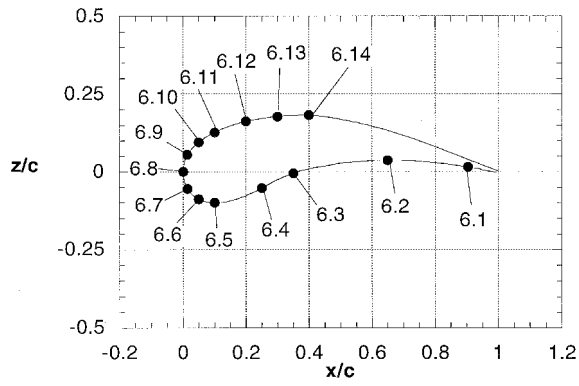

Fig. 4 Location of hot-film sensors on foreflap.

because the wing fuel tank prohibited the installation of flush pressure ports. The pressure belt consisting of thin plastic tubing (0.062 in. o.d./0.028 in. i.d.) was located near wing-buttline (WBL) 336 just inboard of the hot-film belt in the leading-edge region of the main element. In Fig. 3, the main-wing leading-edge geometry and sensor layout are shown. Earlier predictions[8] indicated that relaminarization of the turbulent flow originating at the attachment line of the main element could occur in this region and, therefore, a fairly dense distribution of hot-film sensors was used. Figure 3 reveals that the typical surface spacing of the sensors was about 1 in. in the leading-edge region (note, the chord of the main element is approximately 90 in.). Flush pressure ports were used to measure surface pressure on the foreflap as indicated in Fig. 1. In Fig. 4, the geometry of the foreflap at WBL 324 is depicted and the locations of the hot-film sensors just outboard of this station are marked.

Results and Discussion

Boundary-layer state measurements for the main element and the foreflap have been analyzed and are presented and discussed in this paper. The measurements include hot-film anemometry and surface pressures that indicate both the apparent relaminarization of the upper surface flow in the leading-edge region of the main element and the turbulent contamination of laminar flow in the leading-edge region of the foreflap by wakes emanating from the slat and the main element.

Main Element

In Fig. 5, the pressure distributions for a range of angles of attack are shown for the airplane in the 40-deg flap configuration. Here, the surface pressure distributions are plotted as a function of the nondimensional surface coordinate s/c instead of the nondimensional chordwise coordinate x/c. At this flap setting, slat no. 5 is in the landing position and a gap exists between the trailing-edge region of the slat and the leading-edge region of the main element (Fig. 2). The results show that the maximum pressure point remains relatively stationary ($s/c \approx -0.05$) with increasing angle of attack. Hot-film sensors 4.8–4.10 bracket this region along the lower surface. The upper-surface flow encounters a strongly favorable pressure gradient until $s/c \approx 0.05$ (sensors 5.4–5.5), at which point the first suction peak occurs. Between this point and the second suction peak at $s/c \approx 0.15$ (sensors 5.11–5.12), a dip in the pressure distribution occurs. Infinite swept-wing boundary-layer calculations have shown that the rise in pressure between the two suction peaks is benign such that no laminar separation is predicted (assuming a laminar attachment line) until just downstream of the second peak.[8]

In the angle-of-attack range from 4 to 12 deg, the pressure distribution around the maximum pressure point is relatively insensitive to changes in angle of attack. This insensitivity results in a nearly constant R_{bar} of approximately 350, based on the calculation procedure discussed in Ref. 2. In Ref. 2, the analysis has shown that attachment-line transition did not occur until this R_{bar} value was reached for the flow over the slat. Any laminar flow in the leading-edge region of the main element is contaminated by access panels, slat brackets/actuators, cutouts, as well as the pressure belt that extended from the upper surface trailing edge around the leading edge to the lower surface trailing edge, as mentioned earlier. This surface roughness in combination with the R_{bar} values in excess of 245 caused the attachment line to be turbulent, as indicated by the hot-film signals of sensors 4.8–4.10 for an angle of attack of approximately 7 deg (a typical angle of attack on approach for landing) in Fig. 6.

A segment of the measured signals of sensors 5.1–5.14 during a slow deceleration is depicted in Fig. 7. At the beginning of the sequence (t = 72,195 s), the airplane had an angle of attack of 5.1 deg ($M_\infty = 0.256$, $R_{\bar{c}} = 10.5 \times 10^6$), gradually increasing to 7.8 deg ($M_\infty = 0.238$, $R_{\bar{c}} = 9.7 \times 10^6$) at the end ($t$ = 72,238 s) of the sequence. Because the attachment-line flow was turbulent, turbulent flow could also be expected downstream of the attachment line. However, the signals of sensors 5.1–5.6 (shown in Fig. 7), depict a pattern that changes from transitional at the beginning of the sequence to nearly fully laminar at the end of the sequence. Note the drop in the fluctuations for the signals of sensors 5.1–5.5, and the decrease in the mean value for the signal of sensor 5.6. The drop in fluctuations and the decrease in the mean are indicative of reversion from turbulent to laminar flow. Sensors 5.7–5.14 remained largely turbulent throughout the deceleration. These results appear to indicate that the turbulent boundary-layer flow in the leading-edge region of the main element was relaminarizing under the influence of the strong favorable pressure gradient.

An important parameter when examining reversion from turbulent to laminar flow is the inverse Reynolds number, $K = (U\zeta/\nu)^{-1}$, based on the local inviscid velocity U and the characteristic length $\zeta = U/U'_s$, with U'_s representing the velocity gradient along the inviscid streamline.[9–12] In two-dimensional flows, for $K > 1 \times 10^{-6}$, the first sign of relaminarization is evident in the form of a thickening viscous sublayer, and for $K > 3 \times 10^{-6}$ relaminarization occurs.[12] In Fig. 8, the calculated maximum value of the relaminarization parameter K_{max} and the corresponding α are plotted as a function of time during the slow deceleration. The α curve demonstrates that the deceleration was smooth and continuous from $\alpha = -1.5$ to 11.5 deg. The K_{max} curve shows a trend similar to the α curve, until α = 8 deg, at which angle-of-attack K_{max} levels out at a

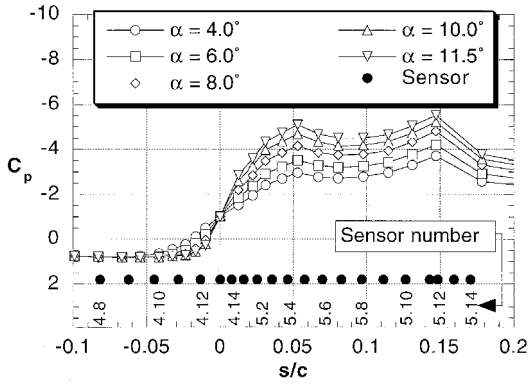

Fig. 5 Location of hot-film sensors and pressure distribution in leading-edge region of main element (40-deg flaps, h_p = 20,000 ft).

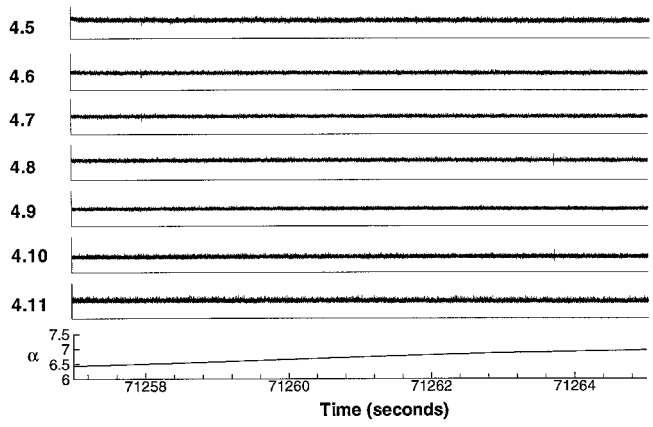

Fig. 6 Hot-film results (digital) measured during slow deceleration, depicting attachment-line state in leading-edge region of main element at $\alpha \approx 7$ deg (40-deg flaps, h_p = 20,000 ft). Segment starts at t = 71,257 s, α = 6.4 deg, $M_\infty = 0.250$, $R_{\bar{c}} = 10.2 \times 10^6$, and ends at t = 71,265 s, α = 7.0 deg, $M_\infty = 0.246$, $R_{\bar{c}} = 10.1 \times 10^6$. Vertical scale range is identical for all sensors.

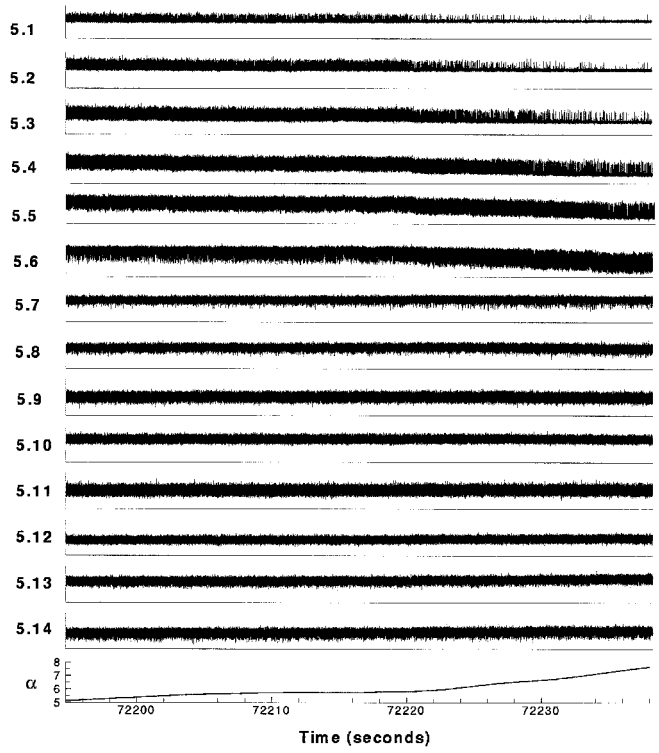

Fig. 7 Hot-film results (digital) measured during slow deceleration depicting boundary-layer state changes in leading-edge region of main element (40-deg flaps, h_p = 20,000 ft). Segment starts at t = 72,195 s, α = 5.1 deg, M_∞ = 0.256, $R_{\bar{c}}$ = 10.5 × 10^6, and ends at t = 72,238 s, α = 7.8 deg, M_∞ = 0.238, $R_{\bar{c}}$ = 9.7 × 10^6. Vertical scale range is identical for all sensors.

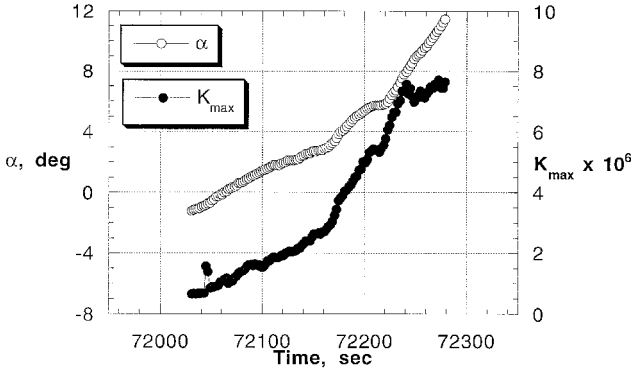

Fig. 8 Variation of airplane angle of attack and maximum relaminarization parameter during slow deceleration (40-deg flaps, h_p = 20,000 ft).

value well in excess of 3 × 10^{-6}, which implies relaminarization.

The intermittency factor γ for each of the hot-film signals over the entire deceleration is plotted in Fig. 9. The parameter K_{max} is also plotted in Fig. 9. Initially, γ = 1 (turbulent flow) for all sensors in the leading-edge region. With increasing time, i.e., increasing α, the intermittency drops to near-zero for sensors 5.1–5.4, where γ = 0 represents laminar flow. Sensors 5.5 and 5.6, located just downstream of the first suction pressure peak (Fig. 5), show a minimum intermittency of 0.1 and 0.2, respectively, whereas sensor 5.7 remained fully turbulent. Changes in intermittency are shown to occur for $K > 1.5 \times 10^{-6}$, in good agreement with previous studies. Correlation of the intermittency factor and the relaminarization parameter also shows that when the K curve levels at t = 72,240 s, the intermittency curves for sensors 5.5 and 5.6 also level out. These data suggest that the relaminarization parameter, as defined earlier, is a valid parameter to predict boundary-layer state reversion for three-dimensional flows with strong favorable pressure gradients.

At a given angle of attack, the increase in intermittency from sensor 5.1–5.4 in the favorable pressure gradient region, observed in the hot-film data of Fig. 7 as well as in the summary plot of Fig. 9, has several possible explanations. One explanation is that by the time the flow reaches sensor 5.1, the turbulence in the boundary layer has not completely decayed across the entire boundary layer. Although the pressure gradient remains favorable, the local K value drops rapidly with increasing distance from the leading edge because of the rise in U and the fact that U^2 appears in the denominator of the expression that defines K. As a result of this drop in K, the level of turbulence in the boundary layer can increase downstream of sensor 5.1. (Note: anemometer data acquisition was limited to two banks of seven sensors each. During the deceleration, the two banks containing sensors 5.1–5.14 were monitored continuously. Consequently, no data could be acquired for sensors 4.1–4.14 of bank 4 during this maneuver.) Another possible explanation for this rise in intermittency is that an external source is contaminating the laminarized boundary layer in the leading-edge region of the main element. These disturbances may originate from the unsteady separated flow in the slat cove just upstream of the main element. In a two-dimensional wind-tunnel investigation of the flowfields in cove regions utilizing a Airbus A300 wing section in the high-lift configuration, Savory et al.[13] measured turbulence levels in excess of 25% in the cove between the slat and the main wing. Depending on the local K level, the main-element boundary layer could be stable or unstable to these external disturbances. Spalart's numerical study[12] of sink-flow boundary layers showed that for $K \geq 1.5 \times 10^{-6}$, the laminar flow is stable to small disturbances. In Fig. 10, a close-up of the hot-film traces of Fig. 7 shows the appearance of turbulent bursts in the relaminarized boundary layer in more detail. If the first expla-

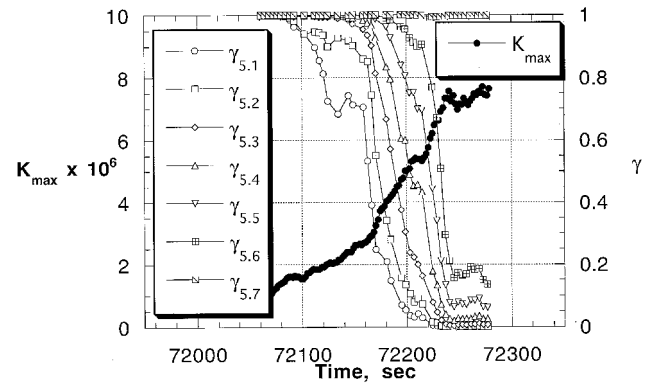

Fig. 9 Correlation between hot-film signal intermittency and relaminarization parameter (40-deg flaps, h_p = 20,000 ft).

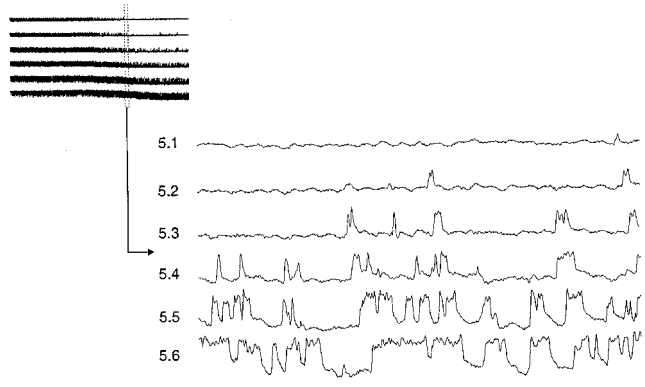

Fig. 10 Close-up of hot-film traces depicting convection of turbulent spots (40-deg flaps, h_p = 20,000 ft).

nation is correct, then these bursts originate from within the boundary layer of the main element and are the result of reemerging turbulence. If the second explanation is correct, then these spots originate from outside the boundary layer (presumably the slat cove), and this turbulent contamination becomes critical at the point where the local K drops below a certain threshold. A third possible explanation for the increase in intermittency is that the relaminarized boundary layer is transitioning as a result of amplification of crossflow instabilities. In Ref. 8, the growth of these instabilities is studied using linear stability theory and flight measured surface pressures for the flow along the upper surface of the main element. The study showed that crossflow-governed transition may occur ahead of the suction peak at these conditions. Further research using hot-wire probes to measure the off-surface flow fluctuations in addition to the surface hot-films is required to explain this flow phenomenon more completely.

Foreflap

In Fig. 4, the geometry of the foreflap at WBL 324 is depicted and the locations of the hot-film sensors just outboard of this station are marked. Earlier studies, e.g., Ref. 8, predicted that extended regions of laminar flow can exist in the leading-edge region of the foreflap, and the present flight experiments confirmed this. Most of the results presented in this section were obtained while the airplane was flying at a constant airspeed (V_i = 140 kn, M_∞ = 0.258, $R_{\bar{c}} = 14.6 \times 10^6$) at h_p = 10,000 ft. During this run, the flap setting was slowly changed from 5 to 40 deg. In Fig. 11, the measured flap angle is plotted as a function of time for the period bracketing the 25-deg flap setting. At this setting, the outboard slat segments (including slat no. 5) move from their takeoff position to their

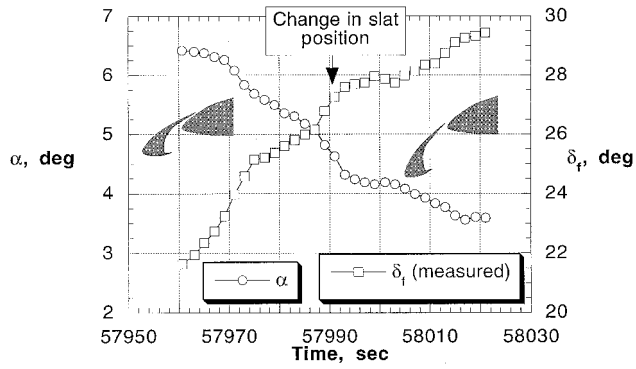

Fig. 11 Variation in angle of attack and flap setting at constant altitude and airspeed (h_p = 10,000 ft, V_i = 140 kn).

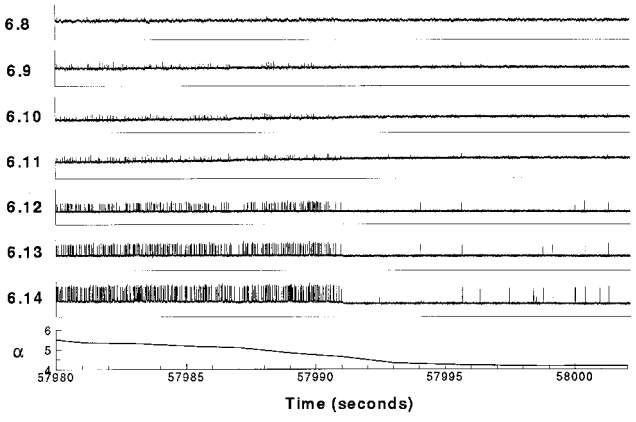

Fig. 12 Hot-film results (digital) depicting turbulent contamination of laminar boundary-layer flow on foreflap (h_p = 10,000 ft, V_i = 140 kn, M_∞ = 0.258, = $R_{\bar{c}}$ = 14.6 × 10⁶). Segment starts at t = 57,980 s, and ends at t = 58,002 s. Vertical scale range is identical for all sensors.

landing position. Note that the measured flap angle differed slightly from the nominal flap setting as a result of flight loads.[13] The change in slat position at t = 57,991 s occurred at a measured flap setting of 27 deg. In Fig. 11, the airplane angle of attack is shown to vary smoothly during this maneuver. The hot-film sensors on the foreflap were located downstream of slat no. 5, and the measured signals for the time period ranging from t = 57,980 to 58,002 s are presented in Fig. 12. There is a dramatic change in the hot-film signals approximately midway, at t = 57,991 s. For t < 57,991 s, the signals of sensors 6.9–6.14 are shown to be laminar with turbulent bursts, whereas for t > 57,991 s, these signals are fully laminar except for an occasional turbulent spike. During this time period, the pressure distribution of the foreflap changed as a result of the increased flap angle, but the change was not significant, as shown in Fig. 13. Closer examination of the hot-film signals indicates that the turbulent bursts appear to be caused by an upstream contamination source; i.e., the slat and/or the main element. In Fig. 14a, a close-up of the signals is shown for t < 57,991 s, and in Fig. 14b, a close-up is shown for t > 57,991 s. In Fig. 14a, note that at one point a sharp turbulent burst first appears on sensor 6.13, and at another point in time a similar type of burst first appears on sensor 6.9. This seems to indicate that the turbulent contamination originating from the slat and/or the main element intersected the foreflap at a slightly oscillating chordwise location. The current data set consisting of surface pressures and hot-film signals is too limited to derive a definitive explanation of the cause of the turbulent contamination on the foreflap. Further research using hot-wire probes upstream of and on the foreflap to measure the off-surface flow fluctuations in addition to the surface hot-films is needed.

Pressure data taken on the main element provide some indication of the possible source of contamination. In Fig. 15, the pressure distribution in the leading-edge region of the main element is presented at t = 57,985 s, just before the change in slat position, and at t = 57,999 s, just after the change in slat position. Downstream of $x/c \approx 0.15$, the pressure distribution of the main element is shown to be nearly unchanged as a result of the change in slat position from the takeoff setting to the landing setting. However, in the leading-edge region of the main element, significant changes occur, including a rise in the maximum pressure coefficient. In Fig. 16, the maximum pressure coefficient is plotted as a function time, and at t = 57,991 s, the pressure coefficient is shown to suddenly increase from 0.56 to 0.74. Assuming infinite swept-wing conditions, the attachment-line pressure coefficient is calculated to be 0.78 (Λ_{le} = 28 deg, M_∞ = 0.26). For t < 57,991 s, much lower pressures were measured in the leading-edge region, indicating that a regular flow-attachment condition didn't exist. It appears that the slat and the main element acted as a single element with a large flow separation bubble, which stretched on the lower surface from the slat cove to the leading-edge region of the

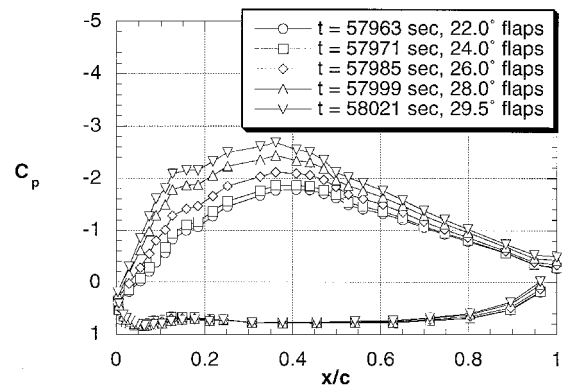

Fig. 13 Effect of flap setting on surface pressures of foreflap (h_p = 10,000 ft, V_i = 140 kn).

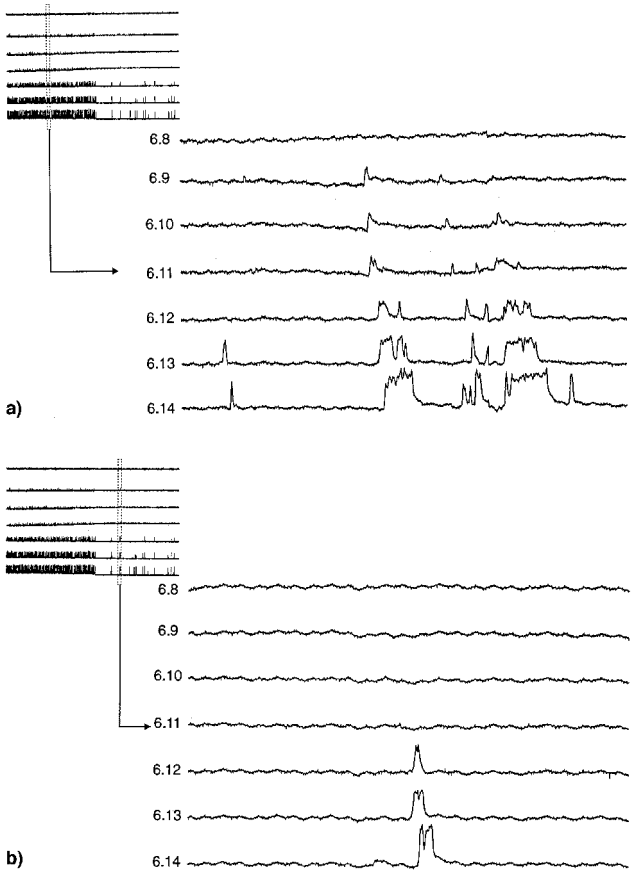

Fig. 14 Close-up of foreflap hot-film traces for a) t < 57,991 s and b) t > 57,991 s (h_p = 10,000 ft, V_i = 140 kn).

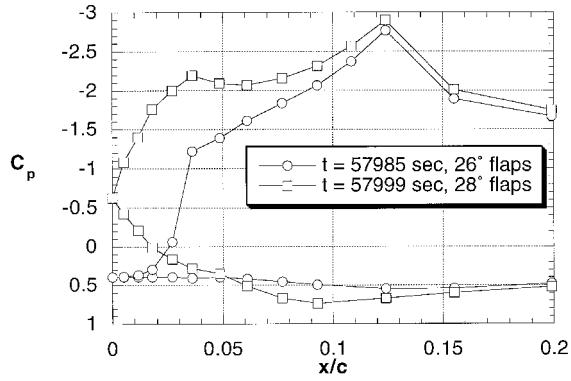

Fig. 15 Effect of flap setting on surface-pressure distribution in leading-edge region of main element (h_p = 10,000 ft, V_i = 140 kn).

main element (Fig. 17a). This separation region shed vorticity, and this vorticity in turn contaminated the laminar flow on the foreflap. For t > 57,991 s, a regular attachment-line condition was approached, indicating that the flow separation zone had shrunk and now was probably contained within the slat cove, as depicted in Fig. 17b. As a result, the shedding was significantly reduced and the contamination on the foreflap virtually disappeared.

This contamination of the flow over the foreflap is not only a function of flap setting but also of angle of attack. In Fig. 18, the maximum pressure coefficient measured in the leading-edge region of the main element during slowly decelerating flight is plotted for a takeoff setting (δ_f = 15 deg) and a landing setting (δ_f = 40 deg). In both cases, the maximum pressure is shown to be relatively low at low angles of attack, indicating that the regular flow-attachment condition didn't exist in the

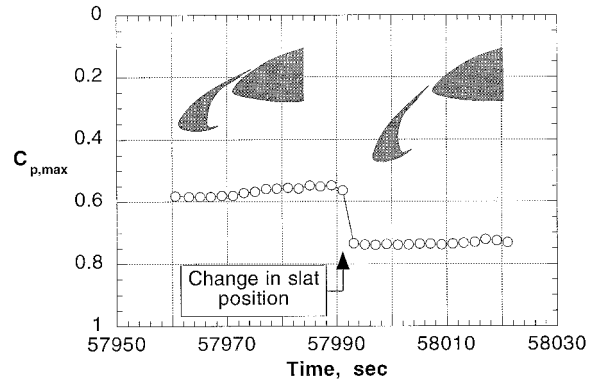

Fig. 16 Effect of flap setting on maximum surface pressure in leading-edge region of main element (h_p = 10,000 ft, V_i = 140 kn).

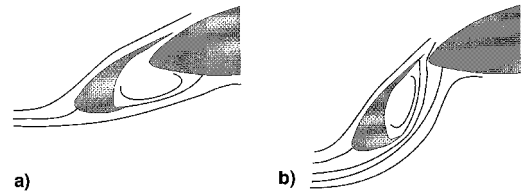

Fig. 17 Sketches of streamline pattern in leading-edge region of main element: a) irregular and b) regular flow-attachment conditions.

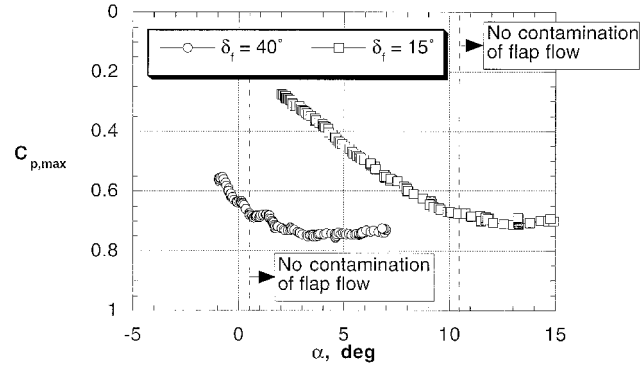

Fig. 18 Effect of flap setting and angle of attack on maximum surface pressure in leading-edge region of main element and on foreflap flow contamination (h_p = 10,000 ft).

leading-edge region of the main element. Simultaneously, all of the sensors on the foreflap indicated significant flow contamination for both flap settings. With increasing angle of attack, the pressure coefficient increased until a relatively constant value commensurate with regular flow-attachment conditions was reached. This occurred at an angle of attack of approximately 2 deg for the 40-deg flap configuration, and at approximately 12 deg for the 15-deg flap configuration. At these conditions, contamination of foreflap flow had virtually disappeared. Figure 18 shows that the maximum pressure coefficient in the leading-edge region of the main element at which clean laminar-flow conditions were measured on the foreflap is approximately 0.65; a value that is bracketed by the maximum pressure coefficients obtained before (flap contamination) and after the change in slat position (no flap contamination) in Fig. 16.

The experimental data presented here and in a companion paper[2] show that extended regions of laminar flow occur not only on single-element wings at cruise conditions but also on multielement wings at high-lift conditions. On the TSRV, the entire slat (except for the cove) experienced laminar flow over a wide angle-of-attack range for all flap settings. In the landing configuration (δ_f > 25 deg), the leading-edge region of the

main element was laminar at medium- to high-lift conditions. The foreflap was typically laminar over at least the initial 40% of the upper surface and the initial 5% of the lower surface. The fact that extended regions of laminar flow on the high-lift elements are achievable and maintainable (at least for this class of transport airplanes) has significant implications in terms of the requirements that should be put on high-lift model testing in ground-based facilities. If the goal of the test is to accurately predict the high-lift characteristics of the full-scale vehicle in flight, then the extent of laminar flow attained in the model test should match that measured in flight.

Concluding Remarks

Flight experiments on NASA Langley Research Center's TSRV (B737-100) airplane have been conducted to document high-lift flow characteristics. Detailed boundary-layer state measurements conducted on the main element and the foreflap are analyzed and presented in this paper.

The hot-film results validate earlier predictions that significant regions of laminar flow can exist on multielement wings at high-lift conditions. In the takeoff configuration ($\delta_f < 25$ deg), the leading edge of the main element is immersed in the separated slat–cove flow for most of the angle-of-attack range, and, consequently, regular flow-attachment conditions are not attained until near-stall conditions. In the landing configuration, this flow problem only exists at very low angles of attack; at regular flow-attachment conditions, the main-element attachment line is turbulent. Under the influence of a strongly favorable pressure gradient in the leading-edge region, the main-element upper-surface flow appears to revert from the turbulent state to the laminar state as measured by the surface hot films. The boundary-layer state reversion in this three-dimensional flow is shown to correlate well with K, calculated along the inviscid streamline. Possible contamination of the relaminarizing boundary layer by the slat–cove separation makes it difficult to determine the exact value of K at which relaminarization occurs. However, changes in the hot-film signals in the leading-edge region are observed for $K > 1.5 \times 10^{6}$. Especially in the takeoff configuration, the cove-flow separation appears also to contaminate the laminar boundary-layer flow on the foreflap. The foreflap contamination is virtually eliminated when regular flow-attachment conditions on the main element are attained as a result of changes in the flap setting or angle of attack. Further research using hot-wire probes to measure the off-surface flow fluctuations, in addition to more closely spaced surface hot films, is required to document more completely the relaminarization and the contamination phenomena.

Acknowledgments

The work by the following authors was supported by the NASA Langley Research Center under Cooperative Agreements NCC1-163 and NCC1-207 (van Dam and Los) and Contracts NAS1-19858 (Miley), NAS1-19864 (Bertelrud), and NAS1-19299 (Vijgen). The authors acknowledge the extraordinary efforts of Keith Harris and Jim Bartlett of the NASA Langley Research Center during the development and installation of the hot-film sensors and anemometry instrumentation.

References

[1]Fiddes, S. P., Kirby, D. A., Woodward, D. S., and Peckham, D. H., "Investigations into the Effects of Scale and Compressibility on Lift and Drag in the RAE 5m Pressurised Low-Speed Wind Tunnel," *Aeronautical Journal*, Vol. 89, March 1985, pp. 93–108.

[2]Van Dam, C. P., Los, S. M., Miley, S. J., Roback, V. E., Yip, L. P., Bertelrud, A., and Vijgen, P. M. H. W., "In-Flight Boundary-Layer State Measurements on a High-Lift System: Slat," *Journal of Aircraft*, Vol. 34, No. 6, 1997, pp. 748–756.

[3]Greff, E., "In-Flight Measurement of Static Pressures and Boundary-Layer State with Integrated Sensors," *Journal of Aircraft*, Vol. 28, No. 5, 1991, pp. 289–299.

[4]Thibert, J. J., "The Garteur High Lift Research Programme," *High-Lift System Aerodynamics*, CP-515, AGARD, Sept. 1993, pp. 16-1–16-21.

[5]Nakayama, A., Stack, J. P., Lin, J. C., and Valarezo, W. O., "Surface Hot-Film Method for the Measurement of Transition, Separation and Reattachment Points," AIAA Paper 93-2918, July 1993.

[6]Kusunose, K., and Cao, H. V., "Prediction of Transition Location for a 2-D Navier-Stokes Solver for Multi-Element Airfoil Configurations," AIAA Paper 94-2376, Jan. 1994.

[7]Yip, L. P., van Dam, C. P., Whitehead, J. H., Hardin, J. D., Miley, S. J., Potter, R. C., Bertelrud, A., Edge, D. C., and Willard, P. E., "The NASA B737-100 High-Lift Flight Research Programme — Measurements and Computations," *Aeronautical Journal*, Vol. 99, Nov. 1995, pp. 372–386.

[8]Van Dam, C. P., Vijgen, P. M. H. W., Yip, L. P., and Potter, R. C., "Leading-Edge Transition and Relaminarization Phenomena on a Subsonic High-Lift System," AIAA Paper 93-3140, July 1993.

[9]Launder, B. E., and Jones, W. P., "On the Prediction of Relaminarization," Aeronautical Research Council, CP 1036, Feb. 1968.

[10]Beasley, J. A., "Calculation of the Laminar Boundary Layer and Prediction of Transition on a Sheared Wing," Aeronautical Research Council, R&M 3787, Oct. 1976.

[11]Narasimha, R., and Sreenivasan, K. R., "Relaminarization of Fluid Flows," *Advances in Applied Mechanics*, edited by Chia-Shun Yih, Vol. 19, Academic, New York, 1979, pp. 221–309.

[12]Spalart, P. R., "Numerical Study of Sink-Flow Boundary Layers," *Journal of Fluid Mechanics*, Vol. 172, 1986, pp. 307–328.

[13]Savory, E., Toy, N., Tahouri, B., and Dalley, S., "The Flow Regimes in the Cove Regions Between a Slat and Wing and Wing and Flap of a Multi-Element Aerofoil," *Engineering Turbulence Modelling and Experiments*, edited by W. Rodi and E. N. Ganic, Elsevier, New York, 1990, pp. 513–522.